Synthesis, X-ray characterization and DFT studies of N-benzimidazolyl-pyrimidine–MIJII) complexes (M = Cu, Co and Ni): the prominent role of π-hole and anion–π interactions

Santiago Cañellas,a Antonio Bauzá,a Aïda Lancho,a Angel García-Raso,*a Joan J. Fiol,a Elies Molins,b Pablo Ballesterc and Antonio Frontera*a

In this manuscript we report the synthesis and X-ray characterization of several complexes of CuIJII), CoIJII) and NiIJII) with 2-IJN-benzimidazolyl)-pyrimidine (L) and nitrate co-ligands. Complexes 1 and 2 are trans and cis isomers, respectively, with formula ijCuL2IJNO3)2]. Furthermore, complexes 2, ijCoL2IJNO3)2] (3) and ijNiL2IJNO3)2] (4) are essentially isostructural with a cis-disposition of the nitrate ligands. In compounds 1–4, the coordination mode of nitrate is terminal bidentate. Finally, during the synthesis of compound 1, a few crystals of a different complex were found and separated manually from the bulk sample and characterized by X-ray diffraction. In this compound (5), the benzimidazole ring of the ligand is oxidized to benzimidazolone (L') and the formula of this unexpected compound is ijCuL'2IJH2O)2]IJNO3)2. Complexes 1 and 5 are characterized by the presence of anion–π interactions that are relevant to the final 3D architecture and packing. In the crystal structures of the five compounds, C–H···O hydrogen bonds, anion–π and π-stacking interactions are described and analysed by means of density functional theory (DFT) calculations since they play an important role in the construction of threedimensional supramolecular frameworks. Moreover, some unconventional interactions have been characterized using Bader's theory of atoms-in-molecules.

Introduction

The chemistry of diazoles, triazoles and related N-containing heterocyclic compounds has been studied with great interest for a long time.1,2 The reason is that such systems play a significant role in many biological processes, due to their ability to coordinate with metal ions.3 For instance, CuIJI)-assisted "click chemistry" was used to assemble diverse triazole compounds containing a peripheral imidazole group, that induced affinity for histamine H4 receptor. Moreover, the utilization of polydentate ligands with sp2-hybridised nitrogen atoms in combination with transition metals originates very interesting inorganic–organic architectures.4 In particular, triazine or pyrimidine moieties attached to one or more pyrazole or triazole rings are clear examples of this strategy.5 The generation of these supramolecular assemblies is accomplished through a variety of cooperative noncovalent interactions. The most common interactions that are usually taken into consideration for the design of multi-component supramolecular assemblies are ion pairing, hydrogen bonding and σ-hole-based7 interactions. Moreover, those involving aromatic systems like π–π stacking,8 cation–π,9 anion–π10 also play a prominent role in supramolecular chemistry. The latter interactions11 have added a new dimension in supramolecular assembly and have emerged as a new concept in aniontransport, anion-sensing and anion-recognition chemistry12 and transmembrane anion transport.13 A new interaction named π-hole has witnessed a resurgent interest in recent times.14 Whilst a σ-hole15 is termed as a region of positive electrostatic potential on the extension of a covalent bond, its counterpart (π-hole)16 is a region of positive electrostatic potential that is perpendicular to a portion of a molecular framework. Positive σ/π-holes interact in a highly directional manner with concentrations of negative charge and competition and interplay between σ/π-holes interactions have been subject to several theoretical investigations.17 Some of us have recently communicated that the interaction of the π-hole found on a nitro group with electron rich entities is energetically favorable and directional.18 In the present study, we report the synthesis and X-ray characterization of several MIJII) coordination complexes containing 2-IJN-benzimidazolyl)- pyrimidine (L) and nitrate as co-ligand, namely cis-ijCuL2IJNO3)2] (1), trans-ijCuL2IJNO3)2] (2), ijCoL2IJNO3)2] (3), ijNiL2IJNO3)2] (4) and ijCuL′ 2IJH2O) 2IJNO3)2] (5) (Scheme 1). The theoretical study is devoted to the analysis of the supramolecular assemblies observed in the solid state of compounds 1–5, giving the possibility of evaluating the different contributions to molecular recognition and of assigning discrete energy values to these contributions. This is an important aspect since this may help to develop energy scoring functions for crystal design. By means of high level DFT calculations and theoretical models we have studied these contributions in the crystal structures that are useful for the understanding of the noncovalent forces and for rationalizing their

influence in the crystal packing paying special attention to the π-hole and anion–π interactions involving the nitrate ligand.

Experimental

Material and measurements

The chemicals and solvents were purchased from commercial sources (Sigma-Aldrich) and were used as received. ESIHRMS was measured in an AutoSpec 3000 using ethanol as solvent and PEG-300 and PEG-600 as calibrant molecules to determine the exact mass. Infrared spectra (KBr pellets) were recorded on a Bruker AMX 300 spectrometer. Proton and carbon chemical shifts in dimethyl sulfoxide solution (DMSO-d6) were referenced to DMSO-d6 itself [1H NMR, δIJDMSO) = 2.50; 13C NMR δIJDMSO) = 39.5 ppm].

Preparation of the compounds

For the preparation of the ligand we have used an improved methodology with respect to the synthetic procedure available in the literature.19 2-IJN-benzimidazolyl)-pyrimidine (L). (70%) A solution of benzimidazole (0.61 g) in 5 ml of anhydrous DMF is added to a cooled (0° C) suspension of NaH (0.25 g, 60% in mineral oil) in 5 ml of anhydrous DMF under argon. The mixture is stirred at 0 °C for 30 min. Then, a solution of 2-chloropyrimidine (0.58 g) in 5 ml of anhydrous DMF is added and the mixture is refluxed for 5 h. The resulting reaction mixture is allowed to reach the room temperature and the solvent is rota-evaporated. The product is purified by adding 40 ml of 0.1 M NaOH and the mixture is stirred for 15 min. The product is filtered off and washed with 40 ml of cold water. Mp (°C): 145–6 (lit. 149–150).19 IR (cm−1): 1570s, 1498s, 1464s, 1440s, 1431s, 1320s, 1299s, 1248s, 1204s, 1003w, 888m, 830s, 793s, 766s, 742s, 640m, 583m, 510m, 424m. 1H NMR, δ(300 MHz; DMSO-d6): 9.08s [1H, C2′ -H], 8.93d [2H, J = 4.8 Hz; C4-H, C6-H], 8.53d [1H, J = 7.8 Hz; C4′ - H], 7.76d [1H, J = 7.8 Hz; C7′ -H], 7.48t [1H, J = 4.8 Hz; C5-H], 7.41t [1H, J = 7.8 Hz, C5′ -H], 7.34t [1H, J = 7.8 Hz, C6′ -H]. 13CNMR, δ(75 MHz; DMSO-d6): 159.81 [C6, C4], 155.95 [C2], 144.97 [C8′], 142.42 [C2′], 131.91 [C9′], 124.99 [C5′], 124.16 [C6′], 120.49 [C7′], 119.55 [C5], 115.88 [C4′].

[CuL2IJNO3)2] (1, trans). (30%) A solution of L, 29.4 mg (0.15 mmol) in 10 ml of CH3CN, is added to a solution of 36.4 mg of CuIJNO3)2·3H2O (0.15 mmol) in 10 ml of CH3CN.

This mixture is refluxed under stirring for 3 hours. The resulting reaction mixture is filtered off and the clear solution is then cooled at room temperature. Suitable green crystals for X-ray diffraction appear at the bottom of the flask after 1–2 days. The green crystals of the Cu complex (2) redissolve if they are allowed to stay in solution for more days and new blue crystals suitable for X-ray diffraction appear at the bottom of the flask after one week, which correspond to complex 1. Selected IR data (cm−1): 3152m, 1595s, 1574s, 1518s, 1484s, 1463vs, 1426vs, 1383s, 1343s, 1302s, 1274s, 1237s, 1014m, 882w, 790m, 764m, 749m, 639w, 591w, 514w, 426w. ESI-HRMS: [CuIJI)IJbimipyr)2]+ (exact mass calc. for C22H16CuN8: 455.0794; found: 455.0798; and [CuIJII)IJNO3)IJbimipyr)2]+ (exact mass calc. for C22H16CuN9O3: exact mass: 517.0672; found: 517.0679). It is well-known that the CuIJII) ions are reduced to CuIJI) during the ESI-HRMS experiment.20 ijCuL2IJNO3)2] (2, cis). (11%) A solution of L, 29.4 mg (0.15 mmol) in 10 ml of CH3CN, is added to a solution of 36.4 mg of CuIJNO3)2·3H2O (0.15 mmol) in 10 ml of CH3CN. This mixture is refluxed under stirring for 3 hours. The resulting reaction mixture is filtered off and the clear solution is then cooled at room temperature. Suitable green crystals for X-ray diffraction appear at the bottom of the flask after 1–2 days. Selected IR data (cm−1): 3142w, 1595w, 1576s, 1504s, 1460s, 1424vs, 1384s, 1337w, 1300s, 1269s, 1233s, 1220m, 1160w, 1114w, 1083w, 1017m, 918w, 890w, 815w, 805w, 790w, 781w, 766m, 750m, 638w, 624w, 590w, 530w, 428w. [CoL2(NO3)2] (3). (63%) A solution of L, 29.4 mg (0.15 mmol) in 10 ml of CH3CN, is added to a solution of 43.6 mg of CoIJNO3)2·6H2O (0.15 mmol) in 10 ml of CH3CN. This mixture is refluxed under stirring for 3 hours and then cooled at room temperature. The resulting reaction mixture is filtered off and the clear solution is kept at room temperature. Suitable purple crystals for X-ray diffraction appear at the bottom of the flask after three days. Selected IR data (cm−1): 3142w, 1595w, 1576s, 1504s, 1460s, 1443m, 1424s, 1384s, 1337m, 1300s, 1273s, 1233s, 1220s, 1162w, 1114w, 1083w, 1017m, 918w, 890w, 817w, 805m, 790w, 781w, 766m, 749m, 698w, 638w, 624w, 590w, 530w, 428w. ESI-HRMS: [Co(NO3)(bimipyr)2]+ (exact mass calc. for C22H16N9O3Co: 513.0708; found: 513.0724) and [Co(NO3)(bimipyr)2(EtOH)]+ (exact mass calc. for C24H22N9O4Co: 559.1127 found: 559.1112).

[NiL2(NO3)2] (4). (64%) A solution of L, 29.4 mg (0.15 mmol) in 10 ml of CH3CN, is added to a solution of 43.6 mg of Ni(NO3)2·6H2O (0.15 mmol) in 10 ml of CH3CN. This mixture is refluxed under stirring for 3 hours and then cooled at room temperature. The resulting reaction mixture is filtered off and the clear solution is kept at room temperature. Suitable green crystals for X-ray diffraction appear at the bottom of the flask after one week. Selected IR data (cm−1): 3142w, 1595w, 1576s, 1504s, 1460s, 1424s, 1384s, 1337m, 1300s, 1266s, 1233s, 1220m, 1163w, 1114w, 1083w, 1017m, 918w, 890w, 817w, 805w, 790w, 781w, 766m, 750m, 638w, 624w, 590w, 530w, 428w.
[CuL′ 2IJH2O)2][(NO3)2] (5). In one experiment, few crystals of this compound were obtained as a minor product during the synthesis of 1 (vide supra). The bulk crystals of 1 (major product) are blue needles and, during its crystallization, a few yellow crystals also appear at the bottom of the vessel that correspond to compound 5. They could be easily separated from the major product manually. This product has been only characterized by X-ray crystallography due to the very small amount of obtained sample. Moreover, after many attempts, we have been unable to reproduce its synthesis, even adding oxidizing agents to the reaction mixture (e.g. bubbling air, H2O2, etc.).

Scheme 1.

X-ray crystallography

The X-ray diffraction data of 2–4 were collected on an Enraf- Nonius CAD4 diffractometer with graphite monochromated Mo-Kα radiation (λ = 0.71073 A). Data collection was performed at room temperature with ω/2θ scans. Data reduction and Lorentz polarization correction were performed with XCAD4.21 The empirical absorption correction implemented in DIFABS was applied.22 The crystal structures were solved by direct methods using SIR2004 (ref. 23) and refined by fullmatrix least-squares on F2 with SHELXL97.24 Non-hydrogen atoms were refined with anisotropic thermal vibration. The crystallographic data for 1 and 5 were collected at 100(2) K on a Bruker Kappa APEX II DUO diffractometer equipped with an APEX 2 4K CCD area detector and a microsource with MoKα radiation (λ = 0.71073 Å). The raw frame data were processed using SAINT and SADABS to yield the reflection data file.25 The structures were solved by direct methods using SIR2011 (ref. 26) and refined on Fo 2 by full-matrix leastsquares procedures, using SHELXL-97. A riding model with the anisotropic thermal vibration fixed at 1.2 times Uiso of the bonded atom was used for the H-atoms. In 5 the same riding model was applied to the H-atoms in the ligand while those in the water molecule were located in the Fourier differences maps and their coordinates refined. The publication material was generated with WinGX.27 Crystal data collection and refinement details are given in Table 1.

Computational details

All calculations were carried out using the TURBOMOLE version 5.9 (ref. 28) using the BP86-D3/def2-TZVP level of theory. To evaluate the interactions in the solid state, we have used the crystallographic coordinates. This procedure and level of theory have been successfully used to evaluate similar interactions. 29 The interaction energies were computed by calculating the difference between the energies of isolated monomers and their assembly. The interaction energies were corrected for the basis set superposition error (BSSE) using the counterpoise method.30 The molecular electrostatic potential (MEP) surfaces have been computed at the B3LYP/6-31+G* level of theory by means of the Spartan software. 31 The “atoms-in-molecules” (AIM)32 analysis was performed at the BP86-D3/def2-TZVP level of theory. The calculation of AIM properties was done using the AIMAll program.33

Results and discussion

Synthesis of the compounds

We have synthesized compounds 1–5 by means of the general procedure shown in Scheme 1. The ligand (L) is easily prepared, in good yield (70%), from sodium benzimidazolate (obtained by treating benzimidazole with NaH) and 2-chloropyrimidine under refluxing conditions in DMF. Dissolution of the ligand in CH3CN and subsequent reaction with Cu, Co or Ni nitrate salts yield the corresponding complexes 1–4, respectively, under refluxing conditions (3 h). Suitable crystals for X-ray diffraction are obtained after 1–7 days at room temperature. Interestingly, the green crystals of the Cu complex (2) redissolve if they are allowed to stay in solution for more days and new blue crystals suitable for X-ray

diffraction appear after one week, which correspond to complex 1. Finally, compound 5, where the ligand is oxidized (L′) was also obtained as a minor product during the synthesis of 1.

Description of the crystal structures

The crystallographic data for compounds 1–5 are shown in Table 1. In addition, selected hydrogen bond parameters are given in Tables 2–3. Crystal structure of CuL2IJNO3)2 (1). The single crystal X-ray diffraction analysis reveals that complex 1 crystallizes in the triclinic system with $P1^{-}$ space group. A perspective view of the complex together with the atom-numbering scheme is shown in Fig. 1. The structure consists of a discrete mononuclear complex where two monodentate ligands coordinate with the copperIJII) center via the imidazolic nitrogen atoms, N(1) in trans-disposition [distance Cu1–N1 = 1.976(2) Å]. Moreover, two nitrate co-ligands are also coordinated with the metal center that sits on the crystallographic inversion center. The coordination mode of the nitrate is anisobidentate [distances Cu1–O1 = 2.020(2) Å and Cu1–O2 = 2.399(2) Å] due to the Jahn–Teller effect.

Table 1.

In the solid state, an interesting assembly is formed by means of self-complementary antiparallel N5–O3 ···N5–O3 interactions [N5···O3i= 2.909(5) Å, i= −x, 1 − y, 1 − z] and anion–π contacts [C1···O3i = 3.084(3) Å, i = −x, 1 − y, 1 − z] involving the C1 atom of the imidazole ring (see Fig. 2). The importance of similar NO3 ···NO3 interactions between coordinated nitrate ligands has been highlighted in the solid state structure of heterobimetallic copperIJII)–uranyl complexes with Schiff-base ligands and nitrate co-ligands.34

Table 2.

Table 3.

Figure 1.

Figure 2.

Moreover, the solid-state structure of complex 1 possesses a remarkable supramolecular architecture through the antiparallel NO3 −···NO3 − and π-stacking interactions (see Fig. 3).

The short π-stacking interactions are established between the electron rich part of the ligand (six membered ring of benzimidazole) and the electron deficient part (either pyrimidine ring or imidazole ring). The most representative contacts that characterize the π-stacking interactions are: C4···C8ii = 3.348(3) and C7···C11iii = 3.240(3) Å (ii = x, y, 1 + z; iii = 1 + x, y, 1 + z). It is remarkably the important role of the NO···NO interaction in the crystal packing since, intuitively, it should be repulsive because of significant charge repulsion between the nitrate ligands. However, since the nitrate anions are coordinated with the Cu2+ metal center, most of the negative charge is transferred to the metal. This interaction is further analysed energetically in the theoretical study
(vide infra). Crystal structures of ML2(NO3)2 (2–4, M = Cu, Co and Ni). The complexes 2–4 are isomorphous and crystallized in monoclinic space group C2/c with the asymmetric unit consisting of half of the complex positioning the metal atom on a twofold axis. The full complex is generated by the symmetry operation of a C2 rotation axis. Perspective view of a representative complex of compounds 2–4 is shown in Fig. 4.

The isostructure of 2–4 consists of a discrete mononuclear complex where two monodentate ligands coordinate with the M(II) center via the imidazolic nitrogen atom N(1) in syn-disposition (see Table 2 for distances). Moreover, two nitrate coligands are also coordinated with the metal center that is located along the C2 symmetry axis. The coordination mode of the nitrato ligands is anisobidentate and the higher anisotropy is found in complex 2 due to the Jahn–Teller effect. As a matter of fact, the M(1) O(1) distance is shorter than M(1)– O(2) in complexes 3 and 4 and the opposite is found in complex
2 (see Table 2).

An interesting assembly observed in the solid state structure of 2–4 is generated by the antiparallel stacking of the aromatic ligands. This stacking is crucial for the final 3D structure and it is shown in Fig. 5. The energetic and geometric features of this π-stacking interaction are further analyzed below (theoretical study). In addition to the stacking interaction, H-bonding interactions between the aromatic

H-atoms and the nitrato ligands are also established and contribute to the overall stabilization energy (vide infra). In Table 3, we summarize the geometric features of the most representative H-bonds and π-stacking interactions for complexes 2–4. In general, the distances that characterize the π-stacking and H-bonding interactions are shorter in complexes 3 and 4 than in 2, apart from the C(14)–H(14)···O(1) interaction that is likely related to the longer M(1)–O(1) coordination bond in 2 due to the Jahn–Teller effect.

Crystal structure of ijCuL′ 2(H2O)2][(NO3)2] (5). The aforementioned complex 5 is formed as a sub-product during the synthesis of compound 1, where the ligand has been oxidized at the C2 position of the five-membered ring. The diagram of compound 5 is shown in Fig. 6. It crystallizes in triclinic space group P1¯ with the asymmetric unit consisting of half of the molecular cation ijCuIIIJL)2IJH2O)2]2+ and one crystallographically independent NO3 − counter-anion. The full system is generated by the symmetry operation of an inversion center where the CuIJII) ion is located. It possesses an octahedral coordination environment whose equatorial plane is formed by the oxygen atom O1 and N3 from the organic ligand and their symmetry related counterparts O1#6 and N3#6 (#6 = 2 − x, 1 − y, 1 − z) from the second ligand. Two water molecules (O2 and O2#6) occupy the trans axial positions. The Cu(1)– O(1) and Cu(1)–N(3) bond distances in the equatorial plane are 1.962(1) and 2.002(1) Å, respectively. The value of the apical Cu(1)–O(2) bond length is 2.345(2) Å, which is longer than the equatorial bond distances.

Figure 3.

Figure 4.

Figure 5.

The solid-state structure of 5 possesses a remarkable supramolecular architecture through a combination of hydrogen bonding and anion–π interactions (see Fig. 7). The NO3 − anion is accommodated through three hydrogen bonds (see Table 4) involving the coordinated water molecules (see blue lines in Fig. 7) and the N1–H group of the ligand (not shown in Fig. 7). Finally, the NO3 − anion also establishes a double anion–π interaction where the N1A atom interacts basically with the benzimidazole part of the ligand (denoted as Aπ1, shortest distance N1A···C6 = 3.223(3) Å] and the O3A atom with the pyrimidinic part of the ligand belonging to another complex [denoted as Aπ2, shortest distance O3A···C9 = 3.173(3) Å]. Antiparallel π–π stacking interactions involving the benzimidazole rings are also relevant in controlling the crystal packing of 5. We have previously reported the ability of similar ligands to participate in antiparallel stacking interactions in protonated N-imidazolyl and N-pyrazolyl derivatives. 19 In the solid state, the combination of the stacking and anion–π interactions forms anion–π/π–π/π–anion assemblies that propagate generating infinite ladders (see Fig. 7) together with the water–nitrate H-bonds. This combination of anion–π/π–π/π–anion interactions has been also observed in bromide salts of terpyridine derivatives35 and protonated aminopyridine with different anions (NO3 − , ClO4 – and PF6 −).36

Figure 6.

Theoretical study

In this part of the manuscript we analyse the interesting and uncommon noncovalent interactions and assemblies observed in the solid state architectures of compounds 1–5 described above. In particular we have mainly focused our attention to the anion–π and π-hole interactions that have been observed in the crystal structures of 1 and 5 and the π-stacking interactions observed in the isostructural complexes 2–4 (vide supra). In an effort to rationalize the anion–π interactions involving the nitrato ligands in 1 and the antiparallel stacking interactions observed in complexes 2–4 (see Fig. 5), we have computed the molecular electrostatic potential surface (MEPS) of complexes 1 and 2 (as an example of the isostructural complexes). From the MEP surfaces some interesting issues arise. First, in both complexes (1 and 2) the most electrostatically positive region (blue color) is located in the molecular plane (aromatic hydrogen atoms) and the most negative electrostatic potential is located in the oxygen atoms of the nitrato ligands thus explaining the number of C–H···O hydrogen bonds (see Table 3). Second, there is also a positive potential isocontour over the six-membered pyrimidinic ring in both complexes (+18 kcal mol−1 in 1 and +24 kcal mol−1 in 2). The MEP value over the five-membered ring of the

benzimidazolic part of the ligand is also positive (+5 kcal mol−1 in 1 and +9 kcal mol−1 in 2). Therefore both rings are well-suited for interacting with electron rich entities. Interestingly, the benzimidazole moiety exhibits a negative potential over the six-membered ring in both complexes (−14 kcal mol−1 in 1 and −9 kcal mol−1 in 2). These results explain the formation of the relevant antiparallel stacking interactions in complexes 1–4 since they are energetically favoured with respect to conventional stacking interactions (e.g. benzene dimer) due to the contribution of electrostatic effects. Moreover, the positive potential over the fivemembered ring of the ligand in complex 1 also explains the formation of the anion–π interaction in the solid state (see Fig. 2). The MEP value over the N atom of the nitrato ligand is negative, therefore the NO···NO interaction is not favored electrostatically. Taking into consideration the short N···O distance, i.e. 2.909(3) Å, this can be considered as an example of the recently described antielectrostatic interactions.37

In compound 1, using the crystallographic coordinates we have evaluated the contribution of the different interactions observed in the solid state. In Fig. 9 we show the fragments and theoretical models used for the calculations. The π-stacking interaction (ΔE1 = −26.6 kcal mol−1) is large and negative due to the antiparallel arrangement of the benzimidazole moiety and the contribution of four C–H···O hydrogen bonds. In an effort to evaluate the contribution of the π-stacking interaction, we have computed a theoretical model (see Fig. 9B) where the two nitrato ligands have been replaced with two hydride ligands. As a result, the interaction energy is reduced to ΔE2 = −16.8 kcal mol−1 that corresponds to the π–π interaction and the difference (ΔE1 − ΔE2 = −9.8 kcal mol−1) is the contribution of the H-bonds. We have also evaluated the anion–π and NO···NO interactions using the X-ray fragment shown in Fig. 8C. The interaction energy is very small (ΔE3 = −4.3 kcal mol−1) likely due to the repulsive contribution of the pseudo-antielectrostatic NO···NO interaction. As a matter of fact, if an additional model is computed (see Fig. 9D) where one nitrato ligand is replaced with a hydride, the interaction energy becomes slightly more favourable (−4.5 kcal mol−1).

In the isostructural compounds 2–4, we have analysed energetically the π–π stacking interactions that are crucial to understand the solid state architecture of these complexes (see Fig. 5). Similar to compound 1, the stacking interactions are in the electrostatically favored antiparallel disposition

Table 4.

Figure 8.

(see Fig. 10). We have computed three theoretical models for each complex to evaluate the strength of the interaction and the results are summarized in Table 5. In the first theoretical model retrieved from the crystal packing, we evaluate the stacking interaction and two C–H···O hydrogen bonds that also participate in the dimer formation (see Fig. 10A, denoted as ΔE4). In order to evaluate the π-stacking interaction without the contribution of the H-bonds, we have used a theoretical model where the two NO3 − ligands have been replaced with the H− ligands (denoted as ΔE4). Finally, we have used a third model where we have eliminated the metal center and the rest of the co-ligands (see Fig. 10C) in order to evaluate the effect of the metal coordination on the π-stacking energy.

From the inspection of the results of Table 5 several issues arise. First, the interaction energies are similar for all complexes indicating that the binding strength is not influenced by the nature of the divalent metal center. Second, the contribution of stacking interaction is approximately −18 kcal mol−1 in the three complexes and it is very similar to the antiparallel stacking interaction computed for complex 1 (ΔE2, see Fig. 9). Finally, the coordination of the ligand with the metal center enhances the π-stacking interaction, since the ΔE6 energies gathered in Table 5 are smaller in absolute value than the ΔE5 ones. This is likely due to the increase in the π-acidity of the five-membered ring upon coordination (higher positive potential over the ring) and, consequently, increasing electrostatic attraction with the electron rich sixmembered ring.

Finally, we have also evaluated energetically the anion–π interactions observed in the solid state of compound 5 (denoted as Aπ1 and Aπ2 in Fig. 7). Since the complex is not neutral, we have used the salt [CuL′ 2IJH2O)2][(NO3)2] in order to evaluate the interactions without the strong contribution of the non-directional ion pair electrostatic effects. Firstly, we

Figure 9.

Figure 10.

have computed the MEP surface of the salt to investigate its binding properties (see Fig. 11). It can be observed that the most positive region of the salt corresponds to the coordinated water molecule (the acidity of the hydrogen atoms of water is enhanced due to the coordination with Cu2+). Moreover, the potential values over the center of pyrimidine and the five-membered ring of benzimidazole are also large and positive (+40 and +35 kcal mol−1, respectively). Finally, the potential over the six-membered ring of benzimidazole is also positive, in contrast to the value observed in complexes 1 and 2 (see Fig. 8), thus it is suitable for interacting with anions.

Table 5.
Figure 11.

Secondly, we have also evaluated the interaction energies of the hydrogen bonding and the anion–π interactions observed in the solid state of 5 by computing the formation energy of the assemblies represented in Fig. 12. We have used the ijCuL′ 2(H2O)2][(NO3)2] salt (A in Fig. 12) as a starting product and evaluated the formation of two different assemblies (B and C in Fig. 12) where the salt interacts with two additional nitrate anions. In each assembly two H-bonding and two anion–π interactions are present. Both assemblies exhibit similar formation energies (ΔE7 = −30.5 kcal mol−1 for B and ΔE8 = −33.8 kcal mol−1 for C) that correspond to the total interaction energy of both type of interactions. In order to evaluate the contribution of the anion–π interactions in both assemblies, we have used additional theoretical models where the coordinated water molecules have been eliminated. The results are included in the bottom of Fig. 12 (D and E). The interaction energy of each Aπ2 (model D) is ½ × ΔE9 = −7.95 kcal mol−1, which is stronger than Aπ1 (model E, ½ × ΔE10 = −5.25 kcal mol−1). This result is consistent with the MEPS analysis that shows larger positive potential over the pyrimidine ring than that over the six-membered ring of the benzimidazole moiety.
Finally, we have used Bader's theory of “atoms-inmolecules”, which provides an unambiguous definition of chemical bonding, to further describe the noncovalent anion–π and NO···NO interactions described above. The AIM theory has been successfully used to characterize and understand a great variety of interactions. In Fig. 13 we show the AIM analysis of the self-assembled dimer of compound 1 and the NO3 —···π contacts in compound 5. As it can be observed

Figure 12.

Figure 13.

for compound 1, each anion–π interaction is characterized by the presence of one bond critical point (red sphere) that connects the oxygen atom with one carbon atom of the imidazole ring. The NO···NO interaction is characterized by the presence of one bond critical point that connects the symmetrically related oxygen atoms of the nitrato ligands thus confirming the existence of the pseudo-antielectrostatic interaction. In compound 5, each anion–π interaction is characterized by the presence of two bond critical points that connect two different oxygen atoms of the nitrate anion with two atoms (C and N) of the benzimidazole moiety. Moreover, the hydrogen bond between the nitrate and the coordinated water molecule is characterized by the presence of one critical point that connects the oxygen atom with the hydrogen atom. The value of the Laplacian of the charge density computed at the bond critical points in both complexes is positive, as is common in closed-shell interactions.

Conclusions

We have synthesized and characterized by X-ray diffraction five N-benzimidazolyl-pyrimidine–M(II) complexes. The solid state structures show that the participation of the organic ligand and anionic co-ligands in concurrent hydrogen bonding, π-hole, π-stacking and anion–π interactions controls the crystal packing. In compound 1, the nitrate anions establish antiparallel NO···NO interactions that have been confirmed using the AIM analysis of critical points and bond paths. This interaction can be considered as an example of the recently defined pseudo-antielectrostatic interactions. In compound 5, the anions have the ability to link the cationic ijCuIJL′)2IJH2O)2]2+ together via anion–π interactions and provide remarkable supramolecular anion–π/π–π/π–anion type network for selfassembly progression. This

experimental investigation supports the role of anion–π and stacking interactions in solidstate chemistry for building multi-dimensional structures. In addition, the computational study highlights the impact of unconventional interaction on the final structure. Finally, the computation of the energetic features of the different noncovalent interactions is important to gain knowledge in the intricate mechanism that governs the molecular recognition and crystal packing and the assignment of discrete energy values to these interactions helps to understand the mechanistic contributions to the crystal engineering community.

Acknowledgements

A.B. and A.F. thank the DGICYT of Spain (projects CTQ2014- 57393-C2-1-P and CONSOLIDER INGENIO 2010 CSD2010-00065, FEDER funds) for financial support. P.B. thanks Gobierno de España MINECO (projects CTQ2014-56295-R and CTQ2011-23014, Severo Ochoa Excellence Accreditation 2014–2018 SEV-2013-0319) and the ICIQ Foundation for funding. We also thank Eduardo C. Escudero-Adán for the X-ray crystallographic data. We thank the CTI (UIB) for the computational facilities.

Notes and references

1 K. D. Karlin, R. W. Cruse, Y. Gultneh, A. Farooq, J. C. Hayes and J. Zubieta, J. Am. Chem. Soc., 1987, 109, 2668–2679; K. D. Karlin, M. S. Haka, R. W. Cruse and Y. Gultneh, J. Am. Chem. Soc., 1985, 107, 5828–5829; N. Kitajima, T. Koda, S. Hashimoto, T. Kitagawa and Y. Moro-oka, J. Am. Chem. Soc., 1991, 113, 5664–5671; N. Kitajima, K. Fujisawa, C. Fujimoto, Y. Moro-oka, S. Hashimoto, T. Kitagawa, K. Toriumi, K. Tatsumi and A. Nakamura, J. Am. Chem. Soc., 1992, 114, 1277–1291; S. W. Lai, T. C. Cheung, M. C. W. Chan, K. K. Cheung, S. M. Peng and C. M. Che, Inorg. Chem., 2000, 39, 255–262; R. A. Ghiladi, T. D. Ju, R. M. Kretzer, P. Moenne- Loccoz, A. S. Woods, R. J. Cotter and K. D. Karlin, J. Inorg. Biochem., 1999, 74, 140–147; T. N. Sorrell and M. L. Garrity, Inorg. Chem., 1991, 30, 210–215; L. Casella, O. Carugo, M. Gullotti, S. Doldi and M. Frassoni, Inorg. Chem., 1996, 35, 1101–1113. 2 A. Volbeda and W. G. L. Hol, J. Mol. Biol., 1989, 209, 249–279; E. I. Solomon, M. J. Baldwin and M. D. Lowery, Chem. Rev., 1992, 92, 521–542; G. M. Brudvig, T. H. Stevens and S. I. Chan, Biochemistry, 1980, 19, 5275–5285; C. T. Martin, R. H. Morese, R. M. Kanne, H. B. Gray, B. G. Mamström and S. I. Chan, Biochemistry, 1981, 20, 5147–5155. 3 D. M. Bassani, J.-M. Lehn, K. Fromm and D. Fenske, Angew. Chem., Int. Ed., 1998, 37, 2364–2367; E. Breuning, M. Ruben, J.-M. Lehn, F. Renz, Y. García, V. Ksenofontov, Ph. Gütlich, E. Weglius and K. Rissanen, Angew. Chem., Int. Ed., 2000, 39, 2504–2507; D. P. Funeriu, J.-M. Lehn, K. M. Fromm and D. Fenske, Chem. – Eur. J., 2000, 6, 2103–2111; A. Frontera, Coord. Chem. Rev., 2013, 257, 1716–1727. 4 J. Elguero, A. Guerrero, F. Gómez de la Torre, A. de la Hoz, F. A. Jalón, B. R. Manzano and A. Rodríguez, New J. Chem., 2001, 25, 1050–1060; S. Chirayil, V. Hedge, Y. Jahng and R. P. Thummel, Inorg. Chem., 1991, 30, 2821–2823; N. Gupta, N. Grover, G. A. Neyhart, P. Singh and H. H. Thorp, Inorg. Chem., 1993, 32, 310–316; F. Gómez de la Torre, A. de la Hoz, F. A. Jalón, B. R. Manzano, A. Otero, A. M. Rodríguez, M. C. Rodríguez-Pérez, A. Echevarría and J. Elguero, Inorg. Chem., 1998, 37, 6606–6614; G. B. Onoa, V. Moreno, M. Font- Bardia, X. Solans, J. M. Pérez and C. Alonso, J. Inorg. Biochem., 1999, 205–212; F. Gómez de la Torre, A. de la Hoz, F. A. Jalón, B. R. Manzano, A. M. Rodríguez, J. Elguero and M. Martínez-Ripoll, Inorg. Chem., 2000, 39, 1152–1162; J. Elguero, A. Fruchier, A. de la Hoz, F. A. Jalón, B. R. Manzano, A. Otero and F. Gómez de la Torre, Chem. Ber., 1996, 129, 589–594. 5 M. Torres, P. Cañellas, C. Estarellas, A. García-Raso, J. J. Fiol, F. M. Albertí, A. Frontera, E. Molins, I. Mata and P. M. Deyà, Tetrahedron, 2012, 68, 2374–2382; P. Cañellas, M. Torres, A. Bauzá, M. M. Cánaves, K. Sánchez, M. I. Cabra, A. García-Raso, J. J. Fiol, P. M. Deyà, E. Molins, I. Mata and A. Frontera, Eur. J. Inorg. Chem., 2012, 3995–4003; F. Orvay, A. Bauza, M. Barcelo-Oliver, A. Garcia-Raso, J. J. Fiol, A. Costa, E. Molins, I. Mata and A. Frontera, CrystEngComm, 2014, 16, 9043–9053. 6 H. J. Schneider, Angew. Chem., Int. Ed., 2009, 48, 3924–3977; J.-M. Lehn, Supramolecular Chemistry, VCH, Weinheim, Germany, 1995; J. W. Steed and J. L. Atwood, Supramolecular Chemistry, Wiley, Chichester, U.K., 2000. 7 J. S. Murray, K. E. Riley, P. Politzer and T. Clark, Aust. J. Chem., 2010, 63, 1598–1607; P. Politzer and J. S. Murray, ChemPhysChem, 2013, 14, 278–294; P. Metrangolo and G. Resnati, Cryst. Growth Des., 2012, 12, 5835–5838; P. Politzer, J. S. Murray and T. Clark, Phys. Chem. Chem. Phys., 2013, 15, 11178; A. Bauzá, T. J. Mooibroek and A. Frontera, Angew. Chem., Int. Ed., 2013, 52, 12317; A. Bauzá and A. Frontera, Angew. Chem., Int. Ed., 2015, 54, 7340–7343. 8 E. A. Meyer, R. K. Castellano and F. Diederich, Angew. Chem., Int. Ed., 2003, 42, 1210; L. M. Salonen, M. Ellermann and F. Diederich, Angew. Chem., Int. Ed., 2011, 50, 4808. 9 J. C. Ma and D. A. Dougherty, Chem. Rev., 1997, 97, 1303; N. Zacharias and D. A. Dougherty, Trends Pharmacol. Sci., 2002, 23, 281. 10 (a) A. Frontera, P. Gamez, M. Mascal, T. J.

Mooibroek and J. Reedijk, Angew. Chem., Int. Ed., 2011, 50, 9564; (b) A. Bauzá, D. Quiñonero, P. M. Deyà and A. Frontera, New J. Chem., 2013, 37, 2636–2641; (c) A. Bauzá, D. Quiñonero, P. M. Deyà and A. Frontera, Chem. Phys. Lett., 2013, 37, 2636–2641. 11 D. Quiñonero, C. Garau, C. Rotger, A. Frontera, P. Ballester, A. Costa and P. M. Deyà, Angew. Chem., Int. Ed., 2002, 41, 3389–3392. 12 (a) A. Frontera, F. Saczewski, M. Gdaniec, E. Dziemidowicz Borys, A. Kurland, P. M. Deyà, D. Quiñonero and C. Garau, Chem. – Eur. J, 2005, 11, 6560–6567; (b) M. Mascal, Angew. Chem., Int. Ed., 2006, 45, 2890–2893; (c) G. Gil-Ramirez, E. C. Escudero-Adan, J. Benet-Buchholz and P. Ballester, Angew. Chem., Int. Ed., 2008, 47, 4114–4118; (d) B. L. Schottel, H. T. Chifotides and K. R. Dunbar, Chem. Soc. Rev., 2008, 37, 68–83; (e) P. Gamez, T. J. Mooibroek, S. J. Teat and J. Reedijk, Acc. Chem. Res., 2007, 40, 435–444; (f) A. Perez-Velasco, V. Gorteau and S. Matile, Angew. Chem., Int. Ed., 2008, 47, 9603–9607; (g) R. E. Dawson, A. Hennig, D. P. Weimann, D. Emeryl, V. Ravikumar, J. Montenegro, T. Takeuchil, S. Gabutti, M. Mayor, J. Mareda, C. A. Schalley and S. Matile, Nat. Chem., 2010, 2, 533–538. 13 (a) V. Gorteau, G. Bollot, J. Mareda, A. Perez-Velasco and S. Matile, J. Am. Chem. Soc., 2006, 128, 14788–14789; (b) V. Gorteau, G. Bollot, J. Mareda and S. Matile, Org. Biomol. Chem., 2007, 5, 3000–3012. 14 M. Solimannejad, V. Ramezani, C. Trujillo, I. Alkorta, G. Sánchez-Sanz and J. Elguero, J. Phys. Chem. A, 2012, 116, 5199–5206. 15 P. Politzer, J. S. Murray and T. Clark, Phys. Chem. Chem. Phys., 2013, 15, 11178–11189; T. Clark, Wiley Interdiscip. Rev.: Comput. Mol. Sci., 2013, 3, 13–20; P. Politzer, J. S. Murray and T. Clark, Phys. Chem. Chem. Phys., 2010, 12, 7748–7757; J. S. Murray, K. E. Riley, P. Politzer and T. Clark, Aust. J. Chem., 2010, 63, 1598–1607; T. Clark, M. Hennemann, J. S. Murray and P. Politzer, J. Mol. Model., 2007, 2, 291–296; A. Bauzá and A. Frontera, Angew. Chem., Int. Ed., 2015, 54, 7340–7343. 16 J. S. Murray, P. Lane, T. Clark, K. E. Riley and P. Politzer, J. Mol. Model., 2012, 18, 541–548. 17 M. Solimannejad, N. Nassirinia and S. Amani, Struct. Chem., 2013, 24, 651–659; M. Esrafili, F. Mohammadian-Sabet and M. Solimannejad, Struct. Chem., 2014, 25, 1197–1205; J. E. Del Bene, I. Alkorta and J. Elguero, J. Phys. Chem. A, 2013, 117, 11592–11604. 18 A. Bauza, T. J. Mooibroek and A. Frontera, Chem. Commun., 2015, 51, 1491–1493; S. Roy, A. Bauza, A. Frontera, R. Banik, A. Purkayastha, M. G. B. Drew, B. M. Reddy, B. Sridhar, S. Kr. Das and S. Das, CrystEngComm, 2015, 17, 3912–3916. 19 M. Torres, P. Cañellas, C. Estarellas, A. García-Raso, J. J. Fiol, F. M. Albertí, A. Frontera, E. Molins, I. Mata and P. M. Deyà, Tetrahedron, 2012, 68, 2374–2382. 20 J. Zhang, V. Frankevich, R. Knochenmuss, S. D. Friess and R. Zenobi, J. Am. Soc. Mass Spectrom., 2003, 14, 42–50. 21 K. Harms and S. Wocadlo, XCAD4, University of Marburg, Marburg, Germany, 1995. 22 N. Walker and D. Stuart, Acta Crystallogr., Sect. A: Found. Crystallogr., 1983, 39, 158–166. 23 M. C. Burla, R. Caliandro, M. Camalli, B. Carrozzini, G. L. Cascarano, L. De Caro, C. Giacovazzo, G. Polidoria and R. Spagna, J. Appl. Crystallogr., 2004, 38, 381–388. 24 G. M. Sheldrick, Acta Crystallogr., Sect. A: Found. Crystallogr., 2008, 64, 112–122. 25 SADABS Bruker AXS, Madison, Wisconsin, USA, 2004; SAINT, Software Users Guide, Version 6.0; Bruker Analytical X-ray Systems, Madison, WI, 1999; G. M. Sheldrick, SADABS v2.03: Area-Detector Absorption Correction, University of Göttingen, Germany, 1999; Saint + Version 7.60A (Bruker AXS 2008); SADABS V. 2008–1 (2008). 26 M. C. Burla, R. Caliandro, M. Camalli, B. Carrozzini, G. L. Cascarano, C. Giacovazzo, M. Mallamo, A. Mazzone, G. Polidori and R. Spagna, J. Appl. Crystallogr., 2012, 45, 357–361. 27 L. J. Farrugia, J. Appl. Crystallogr., 2012, 45, 849–854. 28 R. Ahlrichs, M. Bär, M. Häser, H. Horn and C. Kölmel, Chem. Phys. Lett., 1989, 162, 165. 29 (a) A. Bauzá, A. Terrón, M. Barceló-Oliver, A. García-Rasoand A. Frontera, Inorg. Chim. Acta, 2015, DOI: 10.1016/j. ica.2015.04.028; (b) D. Sadhukhan, M. Maiti, G. Pilet, A. Bauzá, A. Frontera and S. Mitra, Eur. J. Inorg. Chem., 2015, 11, 1958–1972; (c) M. Mirzaei, H. Eshtiagh-Hosseini, Z. Bolouri, Z. Rahmati, A. Esmaeilzadeh, A. Hassanpoor, A. Bauza, P. Ballester, M. Barceló-Oliver, J. T. Mague, Behrouz Notash and A. Frontera, Cryst. Growth Des., 2015, 15, 1351–1361; (d) P. Chakraborty, S. Purkait, S. Mondal, A. Bauzá, A. Frontera, C. Massera and D. Das, CrystEngComm, 2015, 17, 4680–4690. 30 S. F. Boys and F. Bernardi, Mol. Phys., 1970, 19, 553–566. 31 Spartan 10', v. 1.10, Wavefunction Inc, Irvin, CA, USA. 32 R. F. W. Bader, Chem. Rev., 1991, 91, 893–928. 33 T. A. Keith, AIMAll (Version 13.05.06), TK Gristmill Software, Overland Park KS, USA, 2013. 34 S. Ghosh, S. Biswas, A. Bauzá, M. Barceló-Oliver, A. Frontera and A. Ghosh, Inorg. Chem., 2013, 52, 7508–7523. 35 P. Manna, S. K. Seth, A. Bauzá, M. Mitra, S. R. Choudhury, A. Frontera and S. Mukhopadhyay, Cryst. Growth Des., 2014, 14, 747–755. 36 P. Manna, S. K. Seth, A. Das, J. Hemming, R. Prendergast, M. Helliwell, S. R. Choudhury, A. Frontera and S. Mukhopadhyay, Inorg. Chem., 2012, 51, 3557–3571. 37 F. Weinhold and R. A. Klein, Angew. Chem., Int. Ed., 2014, 53, 11214–11217; A. Bauzá, A. Frontera, T. J. Mooibroek and J. Reedijk, CrystEngComm, 2015, 17, 3768–3771.

Scheme 1. Synthetic route to compounds 1-5

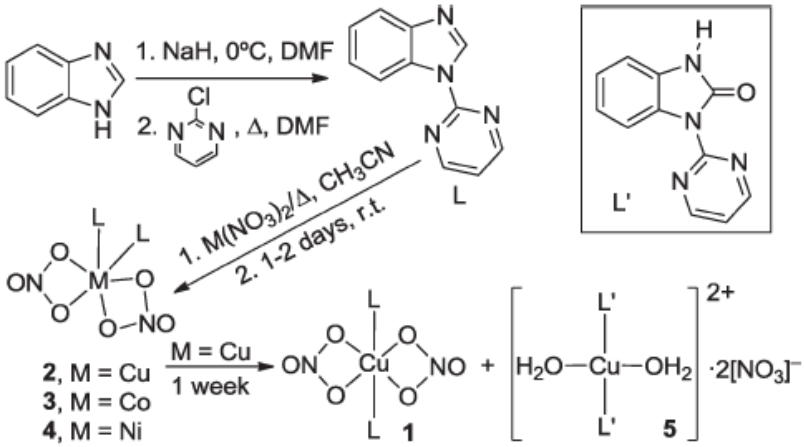

Table 1. Crystallographic data for complexes 1-5

	1	2	3	4	5
Empirical formula	$C_{22}H_{16}CuN_{10}O_6$	$C_{22}H_{16}CuN_{10}O_6$	$C_{22}H_{16}CoN_{10}O_6$	$C_{22}H_{16}NiN_{10}O_6$	$C_{22}H_{20}CuN_{10}O_{10}$
Formula weight	579.99	579.99	575.38	575.16	648.02
Crystal system	Triclinic	Monoclinic	Monoclinic	Monoclinic	Triclinic
Space group	$P\bar{1}$	$C2/c$	$C2/c$	$C2/c$	$P\bar{1}$
Wavelength (Å)	0.71073	0.71073	0.71073	0.71073	0.71073
T (K)	100(2)	293(2)	294(2)	293(2)	100(2)
a (Å)	7.7150(12)	15.354(4)	15.101(6)	15.327(8)	7.0438(7)
b (Å)	8.2580(13)	9.780(2)	9.635(3)	9.623(6)	7.8981(7)
c (Å)	9.5940(16)	16.2709(14)	16.508(8)	16.459(8)	12.0293(11)
α (°)	115.020(5)	90	90	90	81.397(3)
β (°)	92.541(5)	104.57(4)	103.54(6)	2351(2)	89.396(3)
γ (°)	90.020(5)	90	90	90	67.424(3)
Z	1	4	4	4	1
V (Å^3)	553.21(15)	2364.7(9)	2335.1(16)	2335.1(16)	610.18(10)
D_{calc} (Mg m^{-3})	1.741	1.629	1.637	1.625	1.764
μ (mm^{-1})	1.055	0.987	0.799	0.889	0.978
Crystal size	0.10 × 0.07 × 0.01	0.36 × 0.30 × 0.09	0.45 × 0.21 × 0.15	0.39 × 0.09 × 0.09	0.15 × 0.15 × 0.05
F(000)	295	1180	1172	1176	331
Total reflections	6554	4644	2832	3019	5881
Unique reflections	2681	2070	2539	2064	2977
Completeness to θ max (%)	84.7%	99.9%	99.9%	99.9%	87.9%
	$R_{(int)}$ = 0.0409	$R_{(int)}$ = 0.020	$R_{(int)}$ = 0.043	$R_{(int)}$ = 0.069	$R_{(int)}$ = 0.0449
Max. and min. transmission	0.9895 and 0.9019	—	—	—	0.9527 and 0.8672
Data/restraints/parameters	2681/0/178	2070/0/177	2539/0/177	2064/6/177	2977/3/203
θ range (°)	2.35 to 29.72	2.49 to 24.96	2.53 to 26.96	2.52 to 25.24	1.71 to 29.84
Index ranges	$-10 \le h \le 10$	$-17 \le h \le 18$	$-19 \le h \le 18$	$-18 \le h \le 17$	$-9 \le h \le 9$
	$-11 \le k \le 11$	$-11 \le k \le 11$	$0 \le k \le 12$	$0 \le k \le 11$	$-10 \le k \le 10$
	$11 \le l \le 13$	$-19 \le l \le 19$	$0 \le l \le 20$	$0 \le l \le 8$	$0 \le l \le 16$
Goodness-of-fit (GOF) on F^2	1.061	1.079	1.022	0.841	1.059
Final R indices [$I \ge 2\sigma(I)$]	R_1= 0.0442, wR_2= 0.0886	R_1= 0.0389, wR_2= 0.0832	R_1= 0.0451, wR_2= 0.0939	R_1= 0.0925, wR_2= 0.0895	R_1= 0.0480, wR_2= 0.1245
R indices (all data)	R_1= 0.0670, wR_2= 0.0965	R_1= 0.0728, wR_2= 0.0980	R_1= 0.089, wR_2= 0.1055	R_1= 0.2903, wR_2= 0.1299	R_1= 0.0596, wR_2= 0.0480
Largest diff. peak and hole (e Å^{-3})	0.455 and −0.585	0.223 and −0.24	0.253 and −0.243	0.374 and −0.089	0.556 and −0.880

Table 2.

Table 2 Bond distances (Å) and angles (°) of $ML_2(NO_3)_2$ complexes 2–4

Bond	2, M = Cu	3, M = Co	4, M = Ni
M(1)–O(1)	2.352(3)	2.091(2)	2.071(8)
M(1)–O(2)	2.034(3)	2.266(3)	2.188(9)
M(1)–N(1)	1.980(3)	2.040(3)	2.026(10)
O(1)–M(1)–O(2)	57.73(10)	58.08(9)	61.1(3)
O(1)–M(1)–N(1)	108.24(11)	92.80(10)	103.0(4)
O(2)–M(1)–N(1)	93.86(11)	94.13(10)	93.8(4)
O(1)–M(1)–N(1)$^{\#1}$	94.17(10)	107.52(10)	92.9(4)
O(2)–M(1)–N(1)$^{\#1}$	151.88(10)	150.50(9)	153.5(3)
O(1)–M(1)–O(1)$^{\#1}$	146.32(13)	148.49(14)	155.9(5)
O(2)–M(1)–O(2)$^{\#1}$	89.08(15)	85.97(15)	86.6(5)
N(1)–M(1)–N(1)$^{\#1}$	96.44(15)	99.80(14)	97.4(6)

#1: $2 - x, y, \frac{1}{2} - z$.

Table 3.

Table 3 Hydrogen bonds for 2–4 [Å and °]

D–H···A	d(D–H)	d(H···A)	d(D···A)	∠(DHA)
2				
C(9)–H(9)···O(3)$^{\#2}$	0.93	2.60	3.287(5)	131
C(11)–H(11)···O(2)$^{\#3}$	0.93	2.36	3.169(4)	146
C(14)–H(14)···O(1)$^{\#4}$	0.93	2.52	3.399(4)	157
π-stacking (C4···C4$^{\#5}$)	3.469(5)			
3				
C(9)–H(9)···O(3)$^{\#2}$	0.93	2.46	3.223(5)	139
C(11)–H(11)···O(2)$^{\#3}$	0.93	2.32	3.097(4)	140
C(14)–H(14)···O(1)$^{\#4}$	0.93	2.67	3.546(4)	157
π-stacking (C4···C4$^{\#5}$)	3.431(4)			
4				
C(9)–H(9)···O(3)$^{\#6}$	0.93	2.48	3.224(17)	137
C(11)–H(11)···O(2)$^{\#7}$	0.93	2.36	3.120(15)	139
C(14)–H(14)···O(1)$^{\#8}$	0.93	2.65	3.540(15)	161
π-stacking (C4···C4$^{\#5}$)	3.43(2)			

#2: $x, -y, z - \frac{1}{2}$; #3: $-\frac{1}{2} + x, \frac{1}{2} - y, -\frac{1}{2} + z$; #4: $\frac{1}{2} + x, -\frac{1}{2} + y, z$; #5: $2 - x, -y, -z$, #6: $2 - x, -y, -z$; #7: $1.5 - x, \frac{1}{2} - y, -z$; #8: $2.5 - x, y - \frac{1}{2}, \frac{1}{2} - z$.

Figure 1. X-ray structure of compound 1 and the numbering scheme.

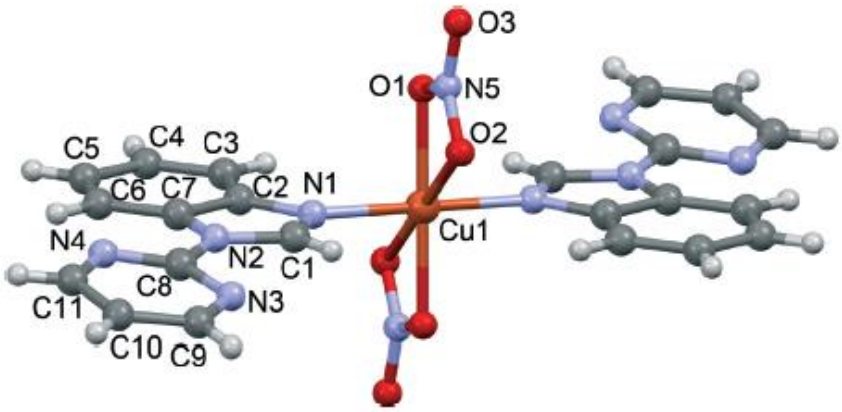

Figure 2. Assembly observed in the X-ray structure of compound 1, with indication of the pi-hole and onion-pi interactions. The distances are in A.

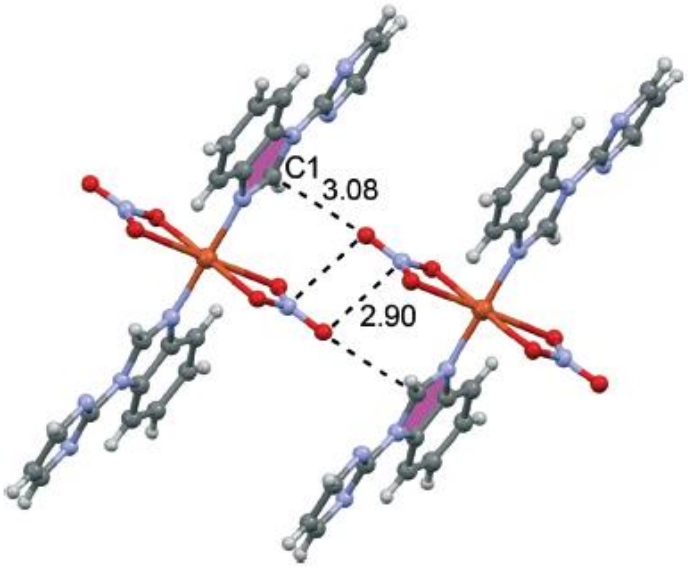

Figure 3. Partial view of the crystal packing of compound 1.

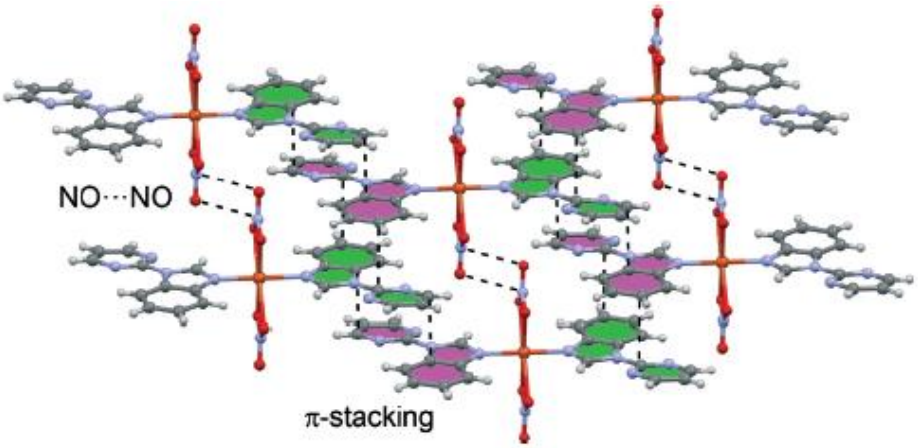

Figure 4. Ball and stick plot of compound 2 and the numbering scheme.

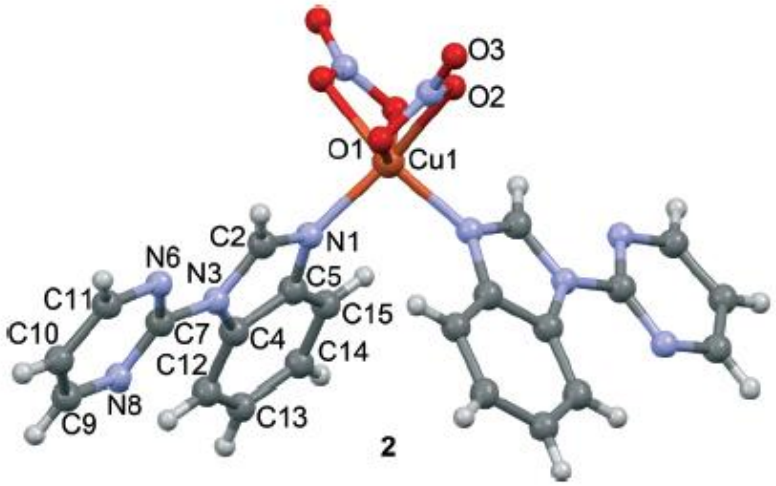

Figure 5.
Pi-Stacking interactions observed in the crystal packing of complexes 2-4. The benzimidazole moiety is represented in CPK format.

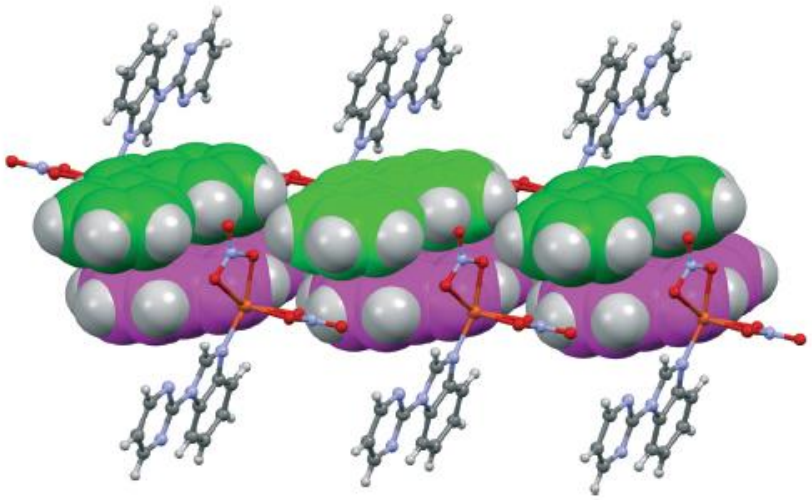

Figure 6. Ball and stick plot of compound 5 and the numbering scheme.

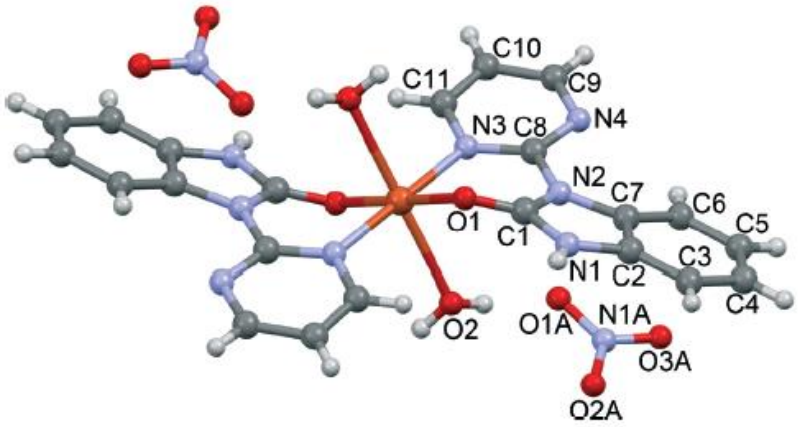

Figure 7. Partial view of the X-ray structure of compound 5. The distances are in A.

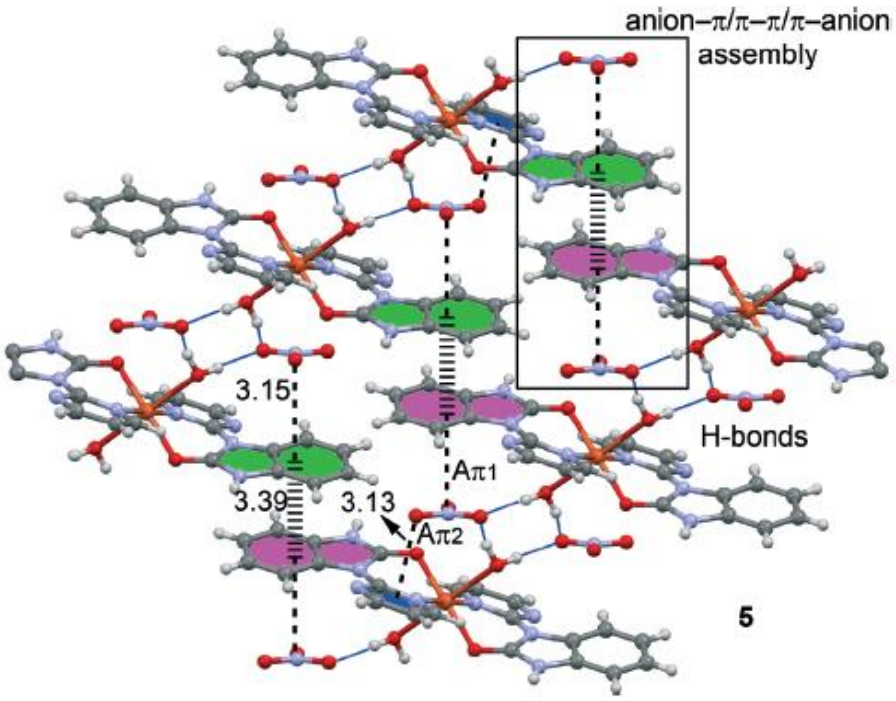

Table 4.

Table 4 Hydrogen bonds for 5 [Å and °]

D–H···A	*d*(D–H)	*d*(H···A)	*d*(D···A)	∠(DHA)
O(2)–H(2O1)···O(1A)	0.83	2.01	2.834(2)	175
O(2)–H(2O2)···O(2A) #9	0.84	2.00	2.807(2)	163
N(1)–H(1)···O(3A) #10	0.86	2.08	2.833(2)	145

#9: $2 - x, -y, 1 - z$; #10: $-1 + x, y, z$.

Figure 8. MEPS surfaces of compounds 1 and 2. The energies in Kcal mol $^{-1}$ are given in selected points of the surfaces.

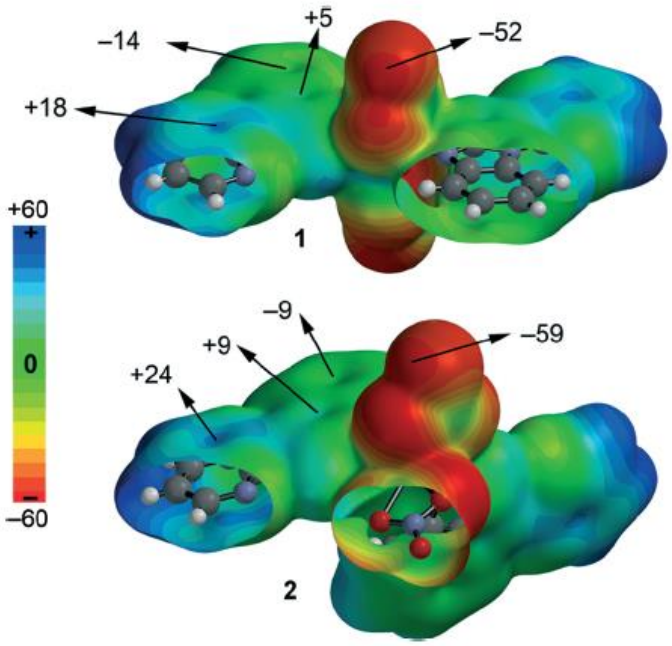

Figure 9.

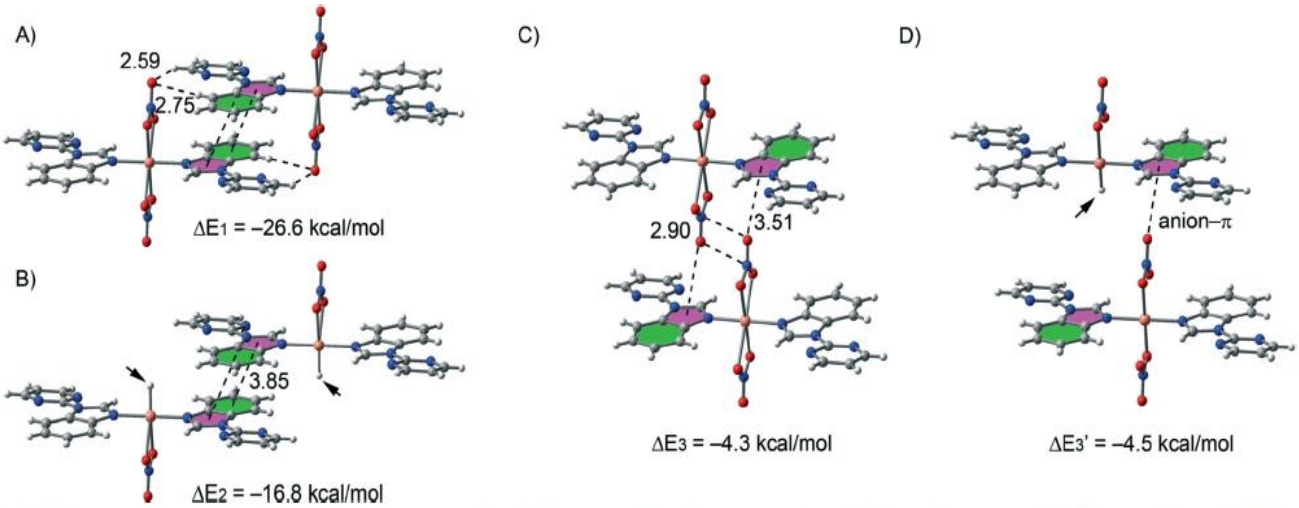

Fig. 9 Theoretical models and binding energies computed to evaluate the noncovalent interactions in compound **1**. The arrows indicate the H^- ligands. $\Delta E_3'$ energy has been multiplied by a factor of two in order to be comparable to ΔE_3.

Figure 10. Theoretical models and binding energies computed to evaluate the noncovalent interactions in compounds 2-4. The arrows indicate the H- ligands. See table 5 for geometric (d) values.

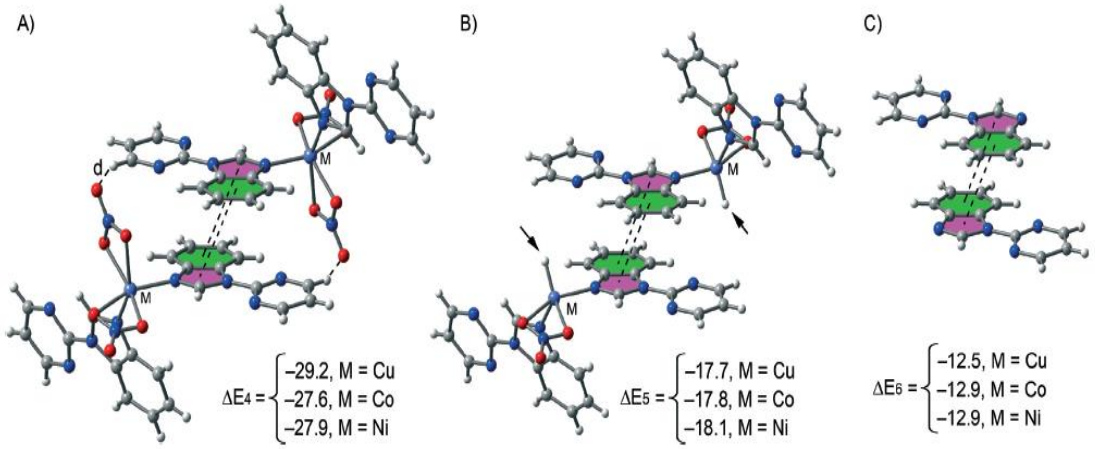

Table 5.

Table 5 Interaction energies (kcal mol^{-1}) with basis set superposition error (BSSE) correction at the BP86-D3/def2-TZVP level of theory for complexes 2–4. See Fig. 10 for the definition of ΔE_{4-6} and d (Å)

Bond	2, M = Cu	3, M = Co	4, M = Ni
ΔE_4	−29.2	−27.6	−27.9
ΔE_5	−17.7	−17.8	−18.1
ΔE_6	−12.5	−12.9	−12.9
d (H-bond)	2.60	2.46	2.48

Figure 11. MEPS surface of compound 5. The energies in kcal mol $^{-1}$ are given in selected points of the surface.

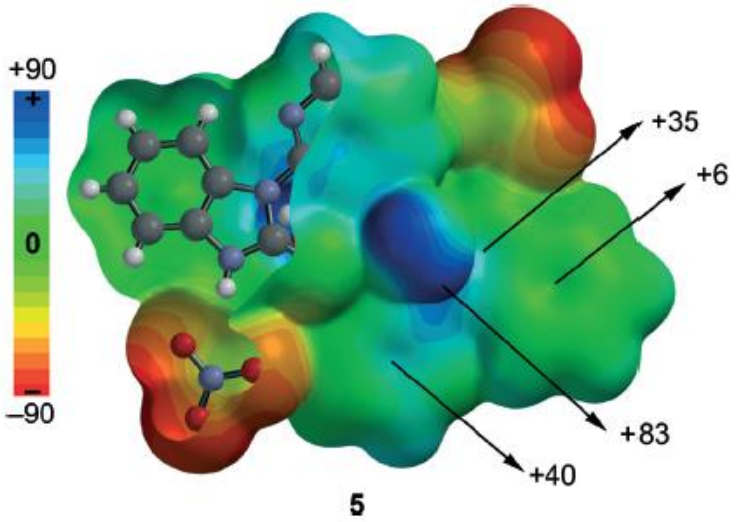

Figure 12. Theoretical models and binding energies computed to evaluate the noncovalent interactions in compound 5.

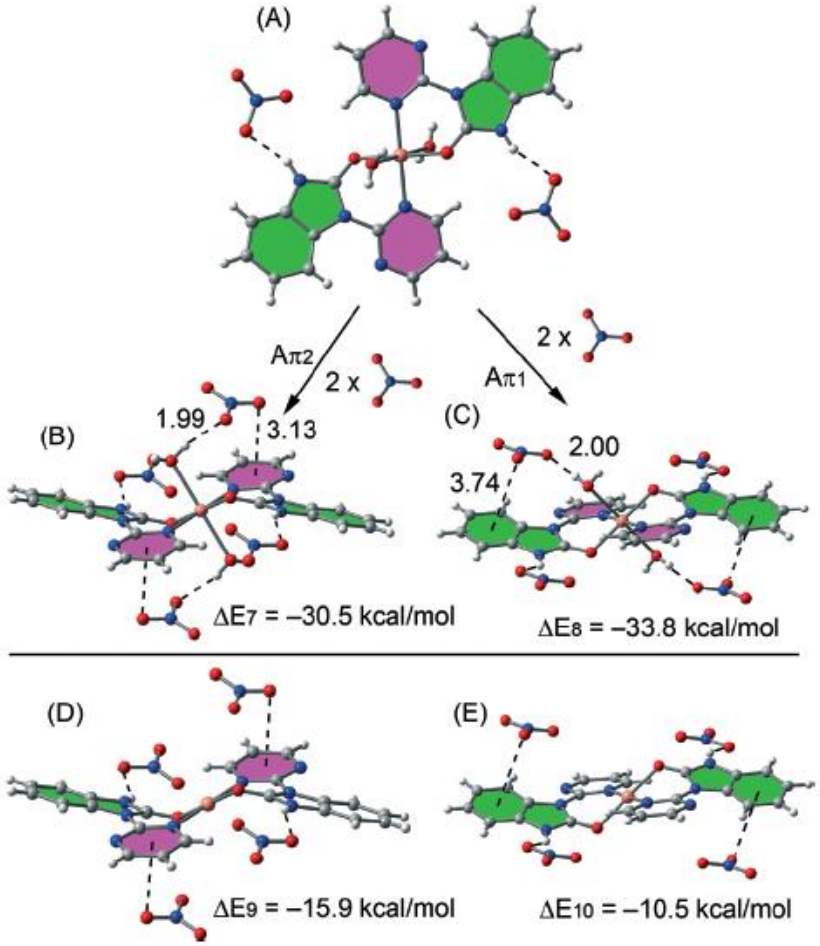

Figure 13. AIM analysis of compounds 1 and 5. Bond, ring and cage critical points are represented by red, yellow and green spheres, respectively. The bond paths connecting bond critical points are also represented by dashed lines.